MOVING DROPLETS - THE MEASUREMENT OF CONTACT LINES

C. POELMA [c], M. FRANKEN, H. KIM, J. WESTERWEEL

Laboratory for Aero & Hydrodynamics (3ME-P&E), Delft University of Technology, The Netherlands
[c] Corresponding author: Tel.: +31-15-2782620; Email: c.poelma@tudelft.nl

KEYWORDS:
Main subjects: contact line dynamics, flow visualization
Fluid: partially-wetting fluid
Visualization method(s): Total Internal Reflection Fluorescence, Tomo-PIV, shadowgraphy
Other keywords: micro/nanoscale, precursor film

ABSTRACT : *Contact lines are the locations where a gas, liquid and a solid meet. From everyday experience we know that such contact lines can be mobile, for example in the case of a water droplet sliding over a glass surface. However, the continuum description of the flow towards or away from a contact line implies that the forces diverge as one approaches a moving contact line. This fundamental problem is of relevance to many applications, and in particular to the development and application of immersion lithography, where a liquid droplet is positioned between the lithographic optical head and the substrate that moves under it. This contribution will address experiments dealing with the shape and stability of a moving droplet and experiments that investigate the underlying behaviour of the nanoscale structure of the moving contact line.*

1 Introduction

Contact lines describe the interface between a gas, liquid and solid. In other words, they define the edge of a droplet on a substrate. From everyday life, we know that these contact lines are mobile, as we can observe rain droplets sliding down a window or the leaf of a plant. If the flow pattern near the contact line is described using a continuum approach a paradox arises: the stress divergence as we approach the contact line, as was described in the landmark work by Huh & Scriven [1]. This is visualized in Figure 1, which schematically shows the streamline patterns in a wedge-shaped model of a steadily moving contact line. Note that the droplet is here assumed stationary, with the solid substrate moving steadily the left. The `kink' in the streamlines requires a diverging stress as we approach the contact line (see Huh & Scriven's work for an analytical result). This stress singularity suggests that the continuum approach is insufficient and additional physical phenomena have to be taken into account [2].

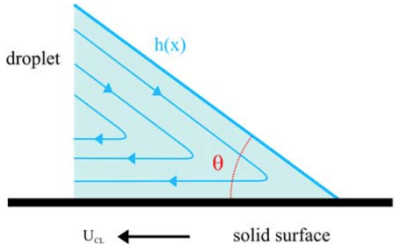

Fig. 1: Schematic flow pattern near a moving contact line (in a reference frame moving with the droplet). [3]

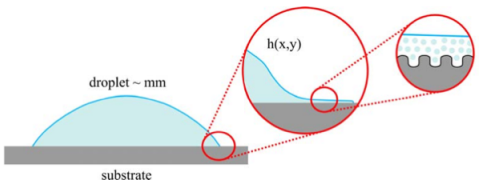

Fig. 2: the precursor film near a contact line (not to scale). [3]

A number of solutions have been proposed to solve this paradox, for instance the relaxation of the `no-slip' condition at the substrate, or the existence of a so-called `pre-cursor film' [4]. The latter is a thin film that precedes a moving contact line (figure 2). Its presence can be attributed to Van der Waals forces and the precursor film results in a more gradual variation of the film height: rather than a wedge with an angle determined by the macroscopic contact angle, this angle is actually variable [4]. Experimental evidence showing the existence of the precursor was given by Hardy in 1919 [5], but to date very little is known about the physical dimensions and behaviour for moving droplets [3]. This is largely due to the very small scales involved: the length of the film is of the order of hundred micrometers, but the thickness is only tens of nanometers.

The study of moving contact lines and precursor film may appear to be a purely academic study to resolve a rather esoteric paradox. However, there are several industrial applications that will directly benefit from a better understanding of moving contact lines, including inkjet printing, coating processes and immersion lithography [6]. In the latter technique, which formed the main motivation for this study, an immersion fluid is placed between an optical head and a substrate (a silicon wafer in the case of semiconductor manufacturing), see also figure 3. The immersion droplet allows the production at a much finer resolution due to the higher refractive index of the immersion fluid compared to air. The immersion hood (which contains the optical head and immersion droplet) has to move to cover the entire substrate, preferably at high velocity to enhance the production ratio. If the velocity exceeds a critical value, the receding droplet interface may become unstable and small droplets may be left behind. Alternatively, air may become trapped in the advancing part of the droplet. Both lead to production loss and should be avoided. A better understanding of the behaviour of contact lines will help optimize this immersion lithography process.

In Section 2 we describe measurements of contact lines at nanoscale, in Section 3 we investigate the macroscopic behaviour of droplets in a model immersion lithography facility.

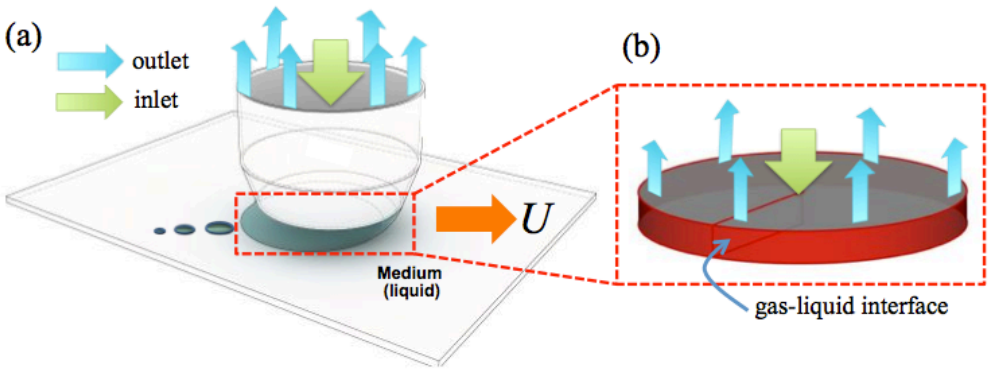

Fig. 3: schematic representation of immersion lithography, showing the droplet of immersion fluid that should stably be positioned between a moving optical head and a substrate. The volume of the droplet is regulated by in-/outflows along the top surface. [7]

2 Nanoscale measurements of moving contact lines

As mentioned above, characterization of the finest details of the contact lines, in particular the precursor film, have been hampered by the fact that the dimensions are of the order of the theoretical limits of imaging resolution - in particular due to the thickness being only tens of nanometers. Side-view shadowgraphy, the standard tool to study macroscopic contact lines, cannot resolve the precursor film. To overcome this, a new quantitative measurement technique was developed, based on total internal reflection fluorescence [8]. Due to the nature of this technique it can measure with a resolution beyond the diffraction limit of the optical system. A drawback is the fact that it cannot simultaneously measure the macroscopic angle, so for a full characterization of a droplet a combination of two techniques is required. The new technique is described in section 2.1 and section 2.2 reports some results that have been obtained.

2.1 Experimental techniques

The measurement technique employed to study the local film height is based on total internal reflection fluorescence (TIRF); it is schematically illustrated in figure 4. A droplet containing a fluorescent dye (Rhodamine 6B) is placed on a glass substrate. It is illuminated from below by means of a laser. The angle of incidence is inclined beyond the critical angle, so that total internal reflection occurs at the transition from glass substrate to the liquid phase of the droplet. The only light that passes this transition is part of an evanescent wave. A key feature of this evanescent wave is the fact that it decays exponentially, with a decay length (*d*) given by the incident angle θ, wavelength λ, and the refractive indices: $d = \lambda/4\pi\ (n_1^2 sin^2\theta - n_2^2)^{-1/2}$. The evanescent wave will trigger a fluorescent signal, which is recorded by a CCD camera from below, through the same objective (60× magnification) that is used for the illumination.

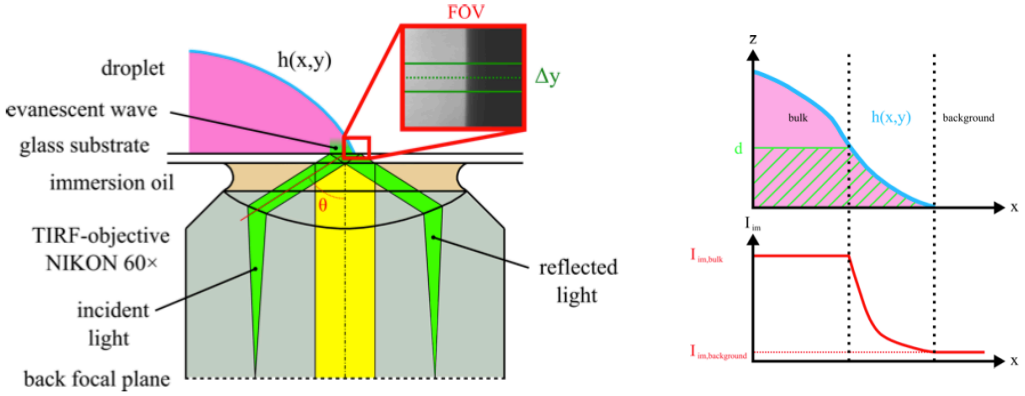

Fig. 4: Film height measurement based on total internal reflection microscopy. The left-hand figure shows the optical set-up to illuminate the droplet near the contact line. The right-hand-side illustrates the relationship between film height and fluorescence intensity. Adapted from Franken [3].

The local recorded fluorescence intensity is given by:

$$I(x,y) = \int_0^\infty C\ I(z)\ dz\ + I_{backgr.} = \underbrace{\int_0^{h(x,y)} C\ I_0\ e^{-z/d}\ dz}_{inside\ droplet} + \underbrace{\int_{h(x,y)}^\infty C\ I_0\ e^{-z/d}\ dz}_{outside\ droplet} + I_{backg.} \qquad (1)$$

The local intensity, described by an integral along the propagation direction of light, has here been split into two contributions (below / above film surface height h). In the equation, C is a lumped parameter describing both the concentration of the fluorescent dye and its efficiency. Outside of the droplet, $C = 0$, so that the second integral in equation 1 is zero. This means that the local intensity $I(x,y)$ observed by the camera can directly be related to the local film height $h(x,y)$:

$$h(x,y) = -d \ ln\left[1 - \frac{I(x,y) - I_{background}}{I_{bulk} - I_{background}}\right] \quad (2)$$

While seemingly straightforward, accurate use of equation 2 to obtain quantitative film heights requires special care. The intensity at the surface (I_0) can be accounted for by measuring in the bulk of a droplet, i.e. away from the contact line. As the local film height is far beyond the penetration depth d of the evanescent wave, the local value of $I_{bulk}(x,y)$ can be determined, which contains I_0. A correction for background noise can be obtained by measuring a region outside of the droplet, far away from the contact line (see figure 4). Note that both I_{bulk} and $I_{background}$ are functions of x and y, to account for non-uniformity in illumination and imaging conditions across the field-of-view. The final parameter required is the value of the penetration depth, d. While refractive indices of the materials and the wavelength are readily available, the accurate determination of the incident angle θ is not trivial in the `through the objective' illumination method. As d is sensitive to this unknown angle ($d \sim 1 / sin\ \theta$), this parameter has to be determined experimentally. This is done by modifying an Atomic Force Microscope (AFM), so that it can be used to carefully traverse a fluorescent tracer particle that is mounted on the AFM scanning tip (see Figure 5). A CCD camera records the image of this particle as it is traversed in the vertical (z) direction. From the (exponential) intensity curve the penetration depth can be determined for the current incident angle; here we find $d = 58 \pm 4$ nm.

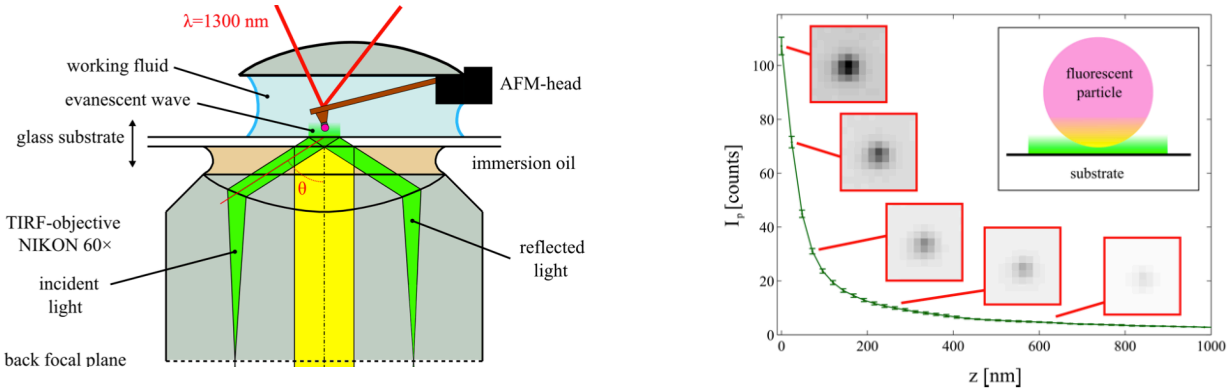

Fig. 5: Determining the penetration depth using a modified AFM head. Left: an AFM head with a fluorescent particle is accurately traversed through the evanescent field in the vertical direction. The images of the particle, captured by a CCD camera, show exponential intensity decay. Modified from Franken [3].

2.2 Results

A first test of the new technique was a validation study, comparing the local film height using TIRF with a reference result. As there are no alternative techniques capable of measuring a highly mobile contact line, this validation was done using a *stationary*, partially wetting droplet of a material suitable for both TIRF measurements and measurements using a scanning AFM in non-contact mode. In the latter technique the AFM oscillates near its resonance frequency. As it approaches the liquid surface,

long or short-range forces will affect the resonance behaviour, so that the presence of the surface can be detected without actually touching the surface. The film height is scanned along the *x*-axis, point-by-point: this makes AFM unsuitable for moving droplets. The results of the validation are shown in figure 6, which shows the local (precursor) film height using both methods; a droplet with a macroscopic contact angle of 8 degrees was used (determined using side-view microscopy). As can be seen, the results from the two methods agree very well. If the film height exceeds the penetration depth (indicated by the dashed line) the signal becomes saturated.

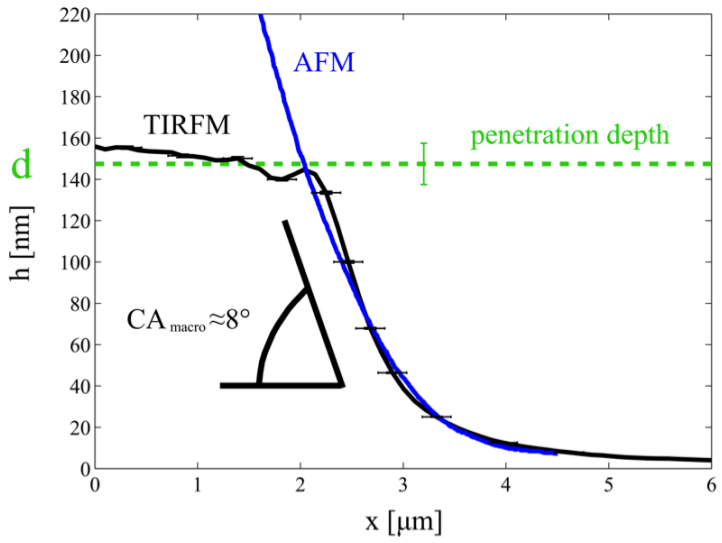

Fig. 6: Validation of the measurement of the film height using total internal reflection, using reference data from an atomic force microscope experiment. Note the difference in *x,h*-axis scales. Adapted from Franken et al. [8].

With the validated method, it is now possible to determine the shape of the precursor film on a moving contact line. Figure 7 shows the precursor film of an advancing contact line of a droplet of glycerol, with a velocity U_{CL} = 11.4 µm/s. As can be seen in the right-hand figure, the film height appears to scale as $h \sim x^{-1/2}$ and has a length of order 100 µm. Similar scaling was found for other contact line velocities (expressed as Capillary number, $Ca = \mu U_{CL}/\gamma$) and other liquids [3].

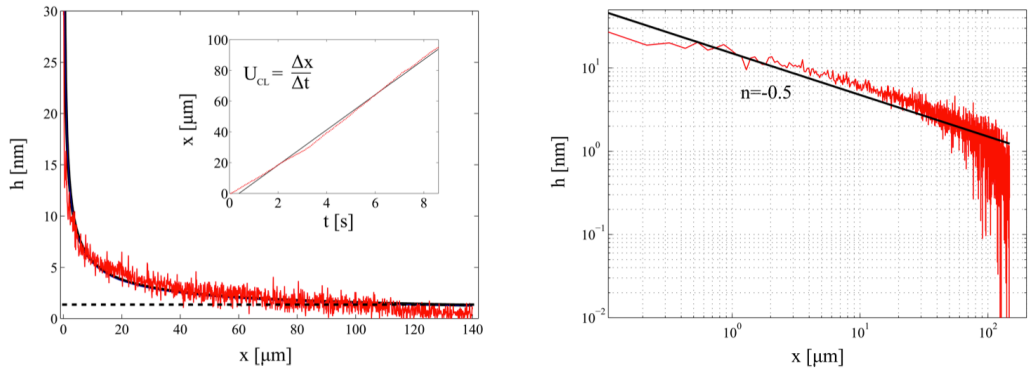

Figure 7: the precursor film of an advancing droplet of glycerol. The inset shows the progression of the contact line, used to determine the contact line velocity. The right-hand side shows the scaling behaviour. [3]

3 Macroscopic droplet behaviour

To understand the macroscopic behaviour of the liquid phase in an immersion lithography process, a model system was constructed [7, 9, 10]. This model system consists of a spinning glass plate and a stationary immersion hood. The radius of this spinning plate, which acts as the substrate, is large enough so that the motion with respect to the hood can be assumed to be uniform. A droplet is placed on top of the substrate and kept in place and at constant volume by means of an immersion needle that contains carefully controlled in- and outflows. Typically, the confined droplet is 200 μm high and 2 mm in diameter. Observation of the shape of the droplet is achieved by both a velocimetry system and by two conventional cameras. The latter two cameras observe the shape of the droplet from below (through the substrate) and from the side. The velocimetry system allows for the measurement of the entire velocity field in the droplet and is described in more detail in section 3.1. The model immersion lithography system is used to observe droplet shape and stability as a function of substrate speed, droplet height and immersion hood design.

3.1 Volumetric velocity measurements

In order to study the velocity field inside the droplet, in particular in the `tail' of the droplet (see Figure 1), a measurement system was constructed to obtain the three-dimensional velocity field. This system consisted of four CCD cameras that image the same field-of-view by means of a set of beam splitters. These cameras image the displacement of fluorescent tracers that are added to the immersion fluid. The data sets can be processed by either 3D particle tracking velocimetry (3D-PTV) or tomographic particle image velocimetry (tomo-PIV). In the PTV approach, particles are first detected in each of the four (2D) images. Triangulation then gives their 3D position within the droplet and they are subsequently matched with the corresponding particles in the next frame. In the tomographic approach, the volumetric grey value distribution of the voxels covering the droplet is first reconstructed using a MART algorithm. Subsequently, 3D cross-correlation is applied to interrogation volumes (here 8×8×8 voxels) to determine the local velocity - i.e. bypassing identification of individual particles. Both methods were compared and gave similar results, with the tomo-PIV method giving a somewhat lower divergence of the velocity [10], which is an estimate of the measurement error.

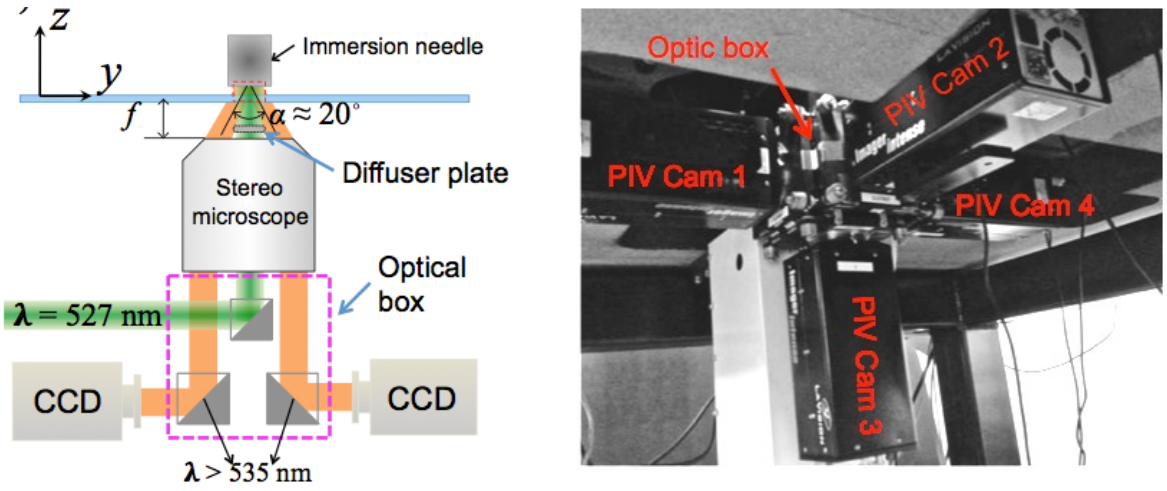

Fig. 8: (Left): schematic representation of the immersion droplet model system, including arrangement of the velocimetry system. (Right) Actual arrangement of the CCD cameras. Adapted from Kim [7].

A typical volumetric velocity field is shown in figure 9. Note that the droplet is stationary (attached to the in/outlet structure of the immersion needle). The bottom moves to the right with a velocity of 1 m/s, resulting in a Reynolds number of 200. Experimental data provided important insight in the flow structure within the droplet, for instance the extent of the influence of the inlet/outflows. The data also confirmed that the velocity field in the `tail' region (far right) is self-similar, providing important cues for the analytical modelling of the shape of the droplet [7].

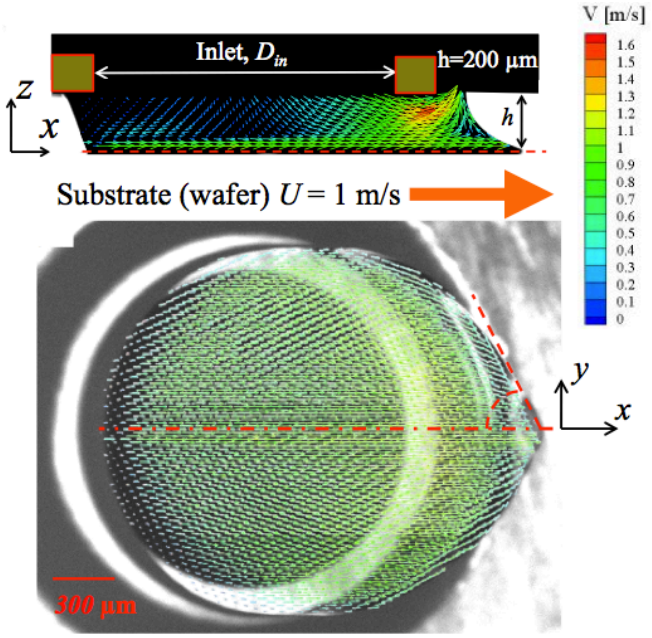

Fig 9.: three-dimensional velocity in the immersion droplet, as measured using tomographic PIV. The top shows a side view at the midplane (note that the substrate moves to the right and the droplet is stationary). The bottom figure shows a bottom view of the droplet at z=10 µm. Reproduced from Kim et al. [10]

3.2 Droplet shape

Velocity measurements such as described in the previous section may provide valuable insight, but they are too time-consuming for extensive parametric studies. Instead, high-speed shadowgraphy was used to investigate the role of the substrate speed and droplet height on the tail length and shape. The substrate is accelerated and the shadowgraphy images are used to determine the two angles that describe the tail shape for each velocity (see also figure 10, which shows the corner angle Φ in the plane parallel to the substrate (xy); the angle θ describes the corresponding angle in the xz-plane). In figure 10, the left-hand side shows the effect of the substrate speed on the droplet shape (shown in bottom view): with increasing substrate the corner angle decreases until break-up occurs. The results for both angles are shown in the right-hand side. The control parameter (the substrate velocity) is expressed as the Capillary number $Ca = \mu U_{CL}/\gamma$. The symbols represent experimental data points (for different surface conditions and droplet volumes). The lines show theoretical models based on lubrication flow; the solid line represents a refined model that could only be formulated with the knowledge obtained from the detailed velocity measurements shown in figure 9 [11].

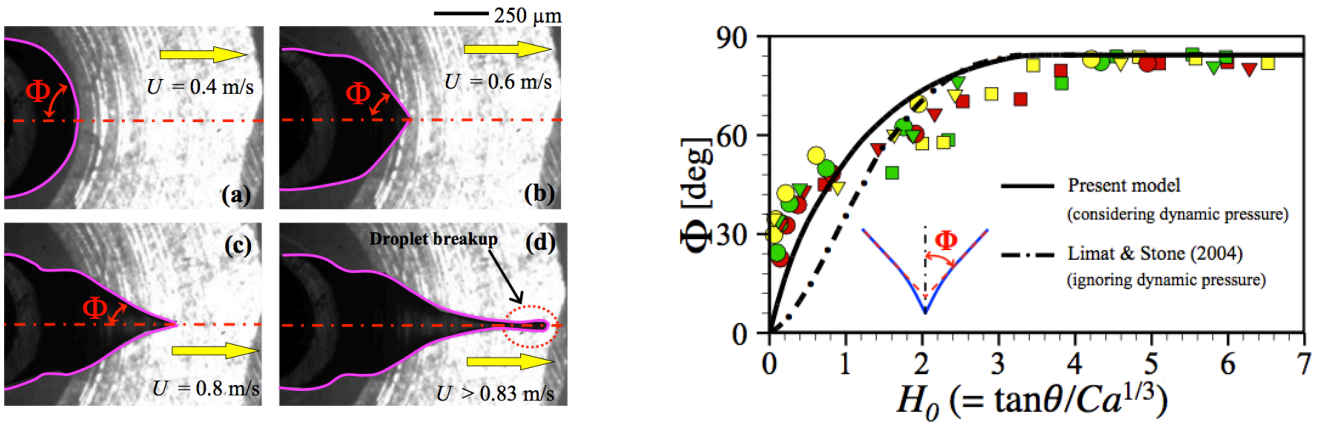

Figure 10: the shape of the tail of the droplet for increasing substrate speed. The left-hand figure shows shadowgraphy images of the droplet for increasing velocity. The right-hand figure shows the relation (experimental and theoretical) between the two angles and velocity. Kim et al. [11]

4 Conclusion and Outlook

Using state-of-the-art optical measurement techniques, we have documented several salient features of droplets moving over a substrate. This ranged from the characterization of the precursor film at the advancing interface, the shape of the tail at the receding end and the flow structure inside the tail. Each result provided a part of the puzzle, but many open questions remain. While better data has already improved our models (see e.g. Figure 10), the exact interaction between nano/microscopic phenomena and macroscopic behaviour is still part of on-going research [3].

Acknowledgements

This work was sponsored by the Industrial Partnership Programme "Contact Line Control during Wetting and Dewetting (CLC)" of the Stichting voor Fundamenteel Onderzoek der Materie (FOM; Foundation for Fundamental Research on Matter), which is financially supported by the Nederlandse Organisatie voor Wetenschappelijk Onderzoek (NWO; Netherlands Organisation for Scientific Research). The CLC programme is co-financed by ASML and Océ.

References

1. Huh C and Scriven LE. Hydrodynamic Model of Steady Movement of a Solid / Liquid / Fluid Contact Line *Journal of Colloid and Interface Science*, Vol. 35, No. 1, 1971, pp. 85-101
2. De Gennes PF. Wetting: statics and dynamics *Rev. Mod. Phys*., Vol. 57, No. 3, 1985, pp.827-863
3. Franken MZF. Dynamics of Precursor Films: Experiment and Theory. *PhD thesis Delft University of Technology* (2014); http://repository.tudelft.nl/view/ir/uuid:4f83a8c0-29ae-4833-b0e2-75ceeabeb12c/
4. Snoeijer J and Andreotti B. Moving Contact Lines: Scales, Regimes, and Dynamical Transitions. *Annual Review of Fluid Mechanics,* Vol. 45, 2013, 2013 pp.269-292
5. Hardy WB. The spreading of fluids on glass. *Philosophical Magazine Series*, Vol. 6, No. 38, 1919, pp.49-55
6. Winkels KG, Peters IR, Evangelista F, Riepen M, Daerr A, Limat L and Snoeijer JH. Receding contact lines: From sliding drops to immersion lithography *The European Physical Journal Special Topics,* Vol.192, No.1, 2011, pp. 195-205
7. Kim H. Moving liquid droplets with inertia: Experiment, simulation, and theory. *PhD thesis Delft University of Technology* (2013); http://repository.tudelft.nl/view/ir/uuid:a9188ceb-e1ff-4233-ae9b-58dd5853ab6d/
8. Franken MZF, Poelma C and Westerweel J. Nanoscale contact line visualization based on total internal reflection fluorescence microscopy. *Optics Express*, Vol. 21, No. 22, pp. 26093-26102 (2013)
9. Kim H, Große S, Elsinga GE and Westerweel J. Full 3D-3C velocity measurement inside a liquid immersion droplet. *Experiments in Fluids* Vol. 51, No. 2, pp. 395-405 (2011)
10. Kim H, Westerweel J and Elsinga GE. Comparison of Tomo-PIV and 3D-PTV for microfluidic flows *Measurement Science & Technology,* Vol. 24, No. 2 024007 (2013)
11. Kim H, Poelma C, Ooms G and Westerweel J. Experimental and theoretical study of dewetting corner flow *submitted* (2014) See also ref. [7]

Copyright Statement